Article

Structural Chemistry & the Design of High-T_c Superconductors

Jeffery L. Tallon

Industrial Research Ltd, and The MacDiarmid Institute for Advanced Materials & Nanotechnology, PO Box 31310, Lower Hutt (e-mail: *J.Tallon@irl.cri.nz*)

About the Author

Jeff Tallon is a Distinguished Scientist and senior research scientist with the High-Temperature Superconductors (HTS) devices group of Industrial Research Ltd. He was named a Companion of the New Zealand Order of Merit in the 2009 Queen's Birthday Honour's List and, in recognition of his work enabling the creation of a new, high-value HTS industry for NZ, was awarded (with Dr Bob Buckley), the inaugural Prime Minister's Science Prize for outstanding achievement in science. Jeff is most well known for his research, beginning in the 1980s, into the highly unusual properties of high-temperature superconductors. He and his colleagues have discovered and patented many novel HTS materials, including the only material currently being developed for cables, magnets, motors and transformers.

Jeff served as Deputy Chair of the Marsden Fund in 1999-2001, introducing the Fast Start programmes for young and emerging researchers, received the Rutherford Medal in 2002 and is currently a member of the National Science Panel that promoted the establishment of the Chief Science Advisor to the Prime Minister.

The essential elements of the structural chemistry of high-T_c superconductors are reviewed and trends and correlations are highlighted, focussing largely but not exclusively on the author's work. Most significant is the contradictory effects of altering ion size and applying external pressure. Increasing ion size stretches the Cu-O bond length and universally increases $T_{c,max}$, while application of pressure increases $T_{c,max}$ and compresses the Cu-O bond. Understanding these contrary observations gets to the heart of the science of high temperature superconductors and enables the design of the optimal superconductor.

Introduction

The International Year of Chemistry is also the centennial of the discovery of superconductivity by Heike Kammerlingh-Onnes at the University of Leiden and it is also 25 years since the discovery of high-temperature superconductors (HTS) by Bednorz and Mueller.[1] Though superconductivity is generally regarded as the domain of physics it is, in fact, intimately associated with synthetic and structural chemistry, and this theme will be developed in the present paper. Kammerlingh-Onnes received the 1913 Nobel Prize, not for the discovery of superconductivity but for the liquefaction of helium, and for about a decade he had a global monopoly on liquid-helium-based cryogenic research. For their part Bednorz and Mueller received the 1987 Nobel Prize – the shortest interval between discovery and award in the history of the Nobels.

It took some 46 years before a theory of conventional low-temperature superconductivity (LTS) was developed. In 1957, Bardeen, Cooper and Schrieffer[2] recognized that interactions between electrons and phonons induce pairs of electrons with opposite momentum to bind into so-called *Cooper pairs*. These singlet pairs, with zero spin, act as bosons and they undergo Bose-Einstein condensation into a ground-state superfluid. In view of this long gap between discovery and developing a successful theory for LTS, perhaps it is not too surprising that we are awaiting still a satisfactory microscopic theory for HTS. Be that as it may, there is still a great deal that we do understand about HTS based on thermodynamics, symmetry, and correlations of physical properties with structure. It is possible, on the basis of these considerations, to design the ideal HTS material and a number of approaches to this central chemical challenge – the optimal structural design of high-temperature superconductors – are outlined.

Structural Chemistry

HTS Cuprates: Defect-Perovskites

The cuprates form structurally-rich families of defect-perovskites with perhaps the only common feature within the families being the square-planar corner-shared sheets of CuO_2 in which the superconductivity originates. These sheets lie in the *ab* plane and are only weakly coupled along the *c*-axis. Such a structure provides what is generally regarded as an essential element in HTS, namely quasi-two-dimensional electron dynamics, which is key to the very high T_c values found in these materials. As a result of this two-dimensionality, it is essential to line up the grains of an HTS conductor in order to make practical wires which will support a large electrical current.

To illustrate both this commonality and diversity in HTS cuprates the structure of three related compounds $YBa_2Cu_3O_{7-\delta}$ (T_c = 93 K), $Y_2Ba_4Cu_7O_{15-\delta}$ (T_c = 97 K) and $YBa_2Cu_4O_8$ (T_c = 80 K) are shown in Fig. 1. These are referred to in shorthand as Y-123, Y-247 and Y-124, respectively. The square-planar CuO_2 sheets lie at the bases of the square pyramids shown in the figure. These planar sheets straddle a bare Y^{3+} ion (small pale grey circles) per unit cell (and in other HTS compounds, a bare Ca^{2+} ion – see Fig. 2 below). These opposing pairs of square pyramids sandwiching Ca or a rare-earth element are a common motif for so-called *bilayer* HTS compounds where each Cu atom is five-coordinated to oxygen. The

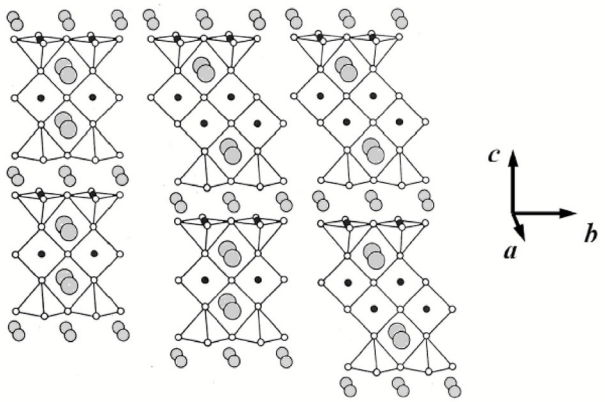

Fig. 1. The structure of Y-123, Y-247 and Y-124, respectively, showing square pyramid oxygen coordination about the planar Cu atoms (small black circles) and linear CuO chains in the *b*-direction; Y-123 has single chains, Y-124 double chains and in Y-247 single and double chains alternate. Large light grey atoms: Ba; small grey: yttrium.

two-sheets within the bilayer are quite strongly coupled while the coupling between successive bilayers is weak.

The ideal perovskite of formula, ABO_3, is cubic with the smaller A^{3+} cation located at the cube corners octahedrally coordinated to six oxygens, while the larger B^{3+} cation is located at the cube centre and is twelve-coordinated to oxygen, four in-plane, four above and four below. In the structures of Fig. 1, Cu adopts the perovskite A position while Y adopts the B position but lacks the four in-plane coordinated oxygens. The cuprates are thus oxygen-deficient perovskites, and they *must* be oxygen deficient since Cu is not trivalent.

Between successive CuO_2 bilayers in the three compounds of Fig. 1 lie one dimensional Cu-O chains extending in the *b*-direction straddled on either side by BaO layers with Ba^{2+} occupying the perovskite B site. Such intermediate layers between the CuO_2 layers are referred to generally as *block layers*. For Y-123 the chains are single CuO chains, for Y-124 they are double Cu_2O_2 chains, and for Y-247 single and double chains alternate. These chain layers can be thought of as square-planar, corner-shared CuO_2 planes with every second row of oxygen atoms absent, again emphasizing that these are oxygen-deficient perovskites. These chains, whether double or single, prove to be very important as they are metallically conducting and they contribute to the superconducting state by what is known as *proximity-induced superconductivity*. They are not intrinsically superconducting but they are induced to be so by their proximity to the naturally superconducting CuO_2 layers.[3]

The double chains of Y-124 (and Y-247) are very stable and remain stoichiometric at all temperatures to compound decomposition (see below). On the other hand, the single chains are not so stable, and when the temperature is raised oxygen diffuses out. When Y-123 and Y-247 are synthesized at high temperature these chains are almost emptied of oxygen, *i.e.* the composition of the chains is $CuO_{1-\delta}$, where δ is close to 1. Under these conditions, Cu in the (empty) chains is monovalent while the Cu in the CuO_2 planes is divalent. Both Y-123 and Y-247 must be slow cooled in oxygen in order to load up these vacant oxygen sites and to allow the oxygens there to order into the extended linear Cu-O chains shown in the figure. Only when δ is reduced to zero, and these chains are well ordered, are these compounds optimized for superconductivity. We secured US, European and Japanese patents for this intermediate compound of formula $Y_2Ba_4Cu_7O_{15-\delta}$ and it has the best intrinsic properties of all HTS cuprates.[4] Unfortunately, no one has succeeded in making a practical conductor out of this material yet – perhaps a task for the future.

The apical oxygen at the apex of the square pyramid is displaced away from the Cu at the base by the Jahn-Teller effect. This lifts the degeneracy of the orbitals, leaving a half filled $d_{x^2-y^2}$ band which is split by the Mott-Hubbard interaction to result in an antiferromagnetic insulator in the undoped state. Doping initiates an insulator-to-metal transition and the onset of superconductivity. It is generally observed that as the Jahn-Teller displacement of the apical oxygen is increased so the maximum observed T_c is also increased.

Homologous Series

A further structural feature of the HTS cuprate families is the tendency to form homologous series with the same *block layer* in each member, but with different numbers of CuO_2 sheets residing between the block layers. Fig. 2 illustrates this for the n = 1, 2 and 3 members of the *BSCCO family* of general formula $Bi_2Sr_2Ca_{n-1}Cu_nO_{2n+4+\delta}$, which we were first to describe.[5] These have single-layer, bilayer and trilayer CuO_2 stacks and, as n is increased by 1, an additional Ca layer and CuO_2 layer are inserted into the structure. The core superconducting $Sr_2Ca_{n-1}Cu_nO_{2n+2}$ sub-stack is a defect perovskite, while the double Bi_2O_2 layer (the two flats sheets of Fig. 2) forms a defect rock salt structure with the in-plane oxygens residing off-centre, closer to the square-planar Bi atoms. Significantly, T_c rises across this series with T_c = 18 K for n = 1, T_c = 95 K for n = 2 and T_c = 110 K for n = 3. It is possible, though very difficult, to make higher homologous members, n = 4, 5, *etc*., but here T_c is found to progressively fall again. Understanding this overall progression is a key challenge in the science of HTS and we will return to the question later.

These compounds are also defect perovskites with a disconcerting array of co-existing defect structures. Typically about 5% of Bi resides on the Sr site; in the n = 2 member Ca and Sr can intersubstitute, though they cannot in the n = 3 member. Excess oxygen (denoted by δ in the formula) resides in interstitial sites between the BiO layer and the SrO layer. Remarkably, they can be located, one by one, using high-resolution scanning tunnelling microscopy.[6] Excess oxygen also resides in the BiO layer,[7] forming an incommensurate structural wave extending in the *b*-direction with periodic bands of Bi^{5+} in perovskite stripes forming a washboard structure with the background rock salt structure comprising Bi^{3+}. So, these materials are structurally and electronically complex, and the unusual defect structures that they exhibit reflect their proximity to several structural and electronic instabilities.

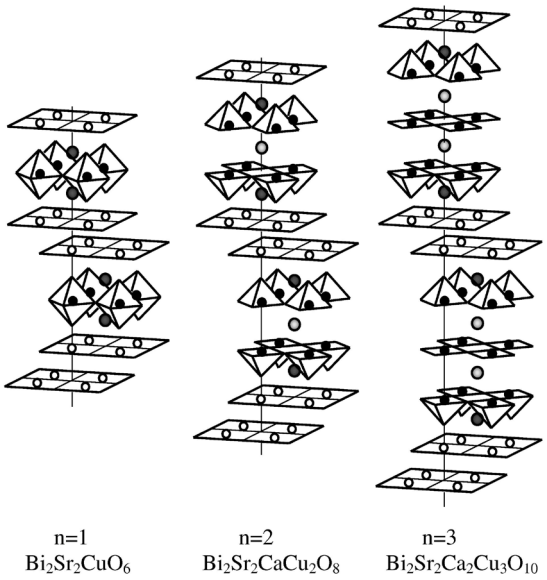

Fig. 2. The homologous structures of $Bi_2Sr_2CuO_{6+\delta}$, $Bi_2Sr_2CaCu_2O_{8+\delta}$ and $Bi_2Sr_2Ca_2Cu_3O_{10+\delta}$, the n = 1, 2 and 3 members of general formula $Bi_2Sr_2Ca_{n-1}Cu_nO_{2n+4+\delta}$ in common shorthand notation, they are referred to as Bi-2201, Bi2212 and Bi-2223 and exhibit T_c values of 18 K, 95 K and 110 K, respectively.

The n = 3 member $Bi_2Sr_2Ca_2Cu_3O_{10+\delta}$ was first identified by our group[5] and was the subject of protracted patent disputes in the USA and Europe over more than a dozen years. Bi-2223 is very slow forming and it takes several weeks to fully react, though synthesis can be accelerated by partial substitution of Pb for Bi.[8] It was this material that was used to make the first generation of HTS wires and we licensed the composition to American Superconductor Corporation. The double Bi_2O_2 layer is weakly bound and, as a consequence, all these BSCCO compounds exhibit a flaky microstructure similar to mica or graphite. Under shear deformation the BiO layers slide over each other such that a simple rolling deformation will align the grains into long extended sheets sharing the same *ab*-plane orientation. Of the approximately 70 known HTS cuprates,[9] BSCCO is the only one in which the grains can be aligned by a rolling deformation, as is needed for a high-current conductor. It is for this reason (combined with its exceptionally high T_c value) that Bi-2223 was quickly established as the only practical HTS conductor for nearly 20 years.

Other homologous cuprate families also exist.[9] The thallium family,[10] of general formula $Tl_2Ba_2Ca_{n-1}Cu_nO_{2n+4+\delta}$, is isostructural with the BSCCO family with Tl-2201 having T_c = 90 K, Tl-2212 having T_c = 118 K and Tl-2223 having T_c = 128 K. Another thallium family has the Tl_2O_2 double layer replaced by a single layer $Tl_{0.5}Pb_{0.5}O$ with members naturally referred to as Tl-1201, Tl-1212 and Tl-1223, *etc*. Their general formula is $Tl_{0.5}Pb_{0.5}Sr_2Ca_{n-1}Cu_nO_{2n+3+\delta}$, Another very important Hg-based family[11] is isostructural with this latter family where $Tl_{0.5}Pb_{0.5}O$ is replaced by a bare Hg, *i.e*. the oxygen in the layer is removed. This has the general formula $HgBa_2Ca_{n-1}Cu_nO_{2n+2+\delta}$, and the n = 3 member, $HgBa_2Ca_2Cu_3O_{8+\delta}$, exhibits the highest T_c known amongst the cuprates (135 K under ambient pressure and 165 K under high pressure). Again, the Hg family exhibits a rise then fall in T_c as n increases (T_c = 95 K, 125 K, 135 K and 128 K for n = 1, 2, 3 and 4, respectively).

Phase Diagrams

Electronic Phase Diagram

The cuprates exhibit a universal phase diagram with doping and, to illustrate, the single-layer compound $La_{2-x}Sr_xCuO_4$ is considered. When x = 0 the parent compound La_2CuO_4 is an undoped antiferromagnetic (AF) insulator, as noted above. Substitution of Sr^{2+} for La^{3+} removes electrons from the hybridized Cu-O orbitals, and thus dopes in holes. The doped hole concentration, p, is just $p = x$. In other cuprates, subject to thermodynamic and chemical constraints, hole doping can be achieved by similar altervalent cation substitutions or by increasing the oxygen content. Importantly, the cuprates seem to display a common phase diagram when T_c is scaled by its maximum value in the phase curve, $T_{c,max}$. A schematic representation of the generic phase diagram is shown in Fig. 3.[12,13]

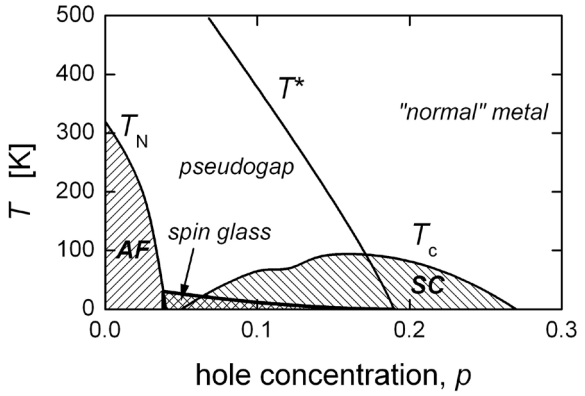

Fig. 3. The universal phase diagram for hole-doped HTS superconductors showing a region of AF ordering at low p and superconductivity (SC) at higher doping. Optimal doping, where $T_c = T_{c,max}$, occurs at p = 0.16 holes/Cu. The *overdoped region* corresponds to $p > 0.16$ while the *underdoped region* corresponds to $p < 0.16$. Short-range AF correlations occur in a region below T^*, known as the *pseudogap* state, and these compete with SC below T_c. The pseudogap energy scale $T^* = E_g/k_B$ falls to zero at critical doping $p_{crit} = 0.19$, which may be a quantum critical point. There is a spin-glass state at intermediate doping and the system progresses towards a *normal* metal at high doping.

Long ago we showed that the generic T_c(p) phase curve followed the universal parabola:[14]

$$T_c = T_{c,max}\,[1 - 82.6\,(p\text{-}0.16)^2] \qquad \text{(Eq. 1)}$$

although this ignores the small plateau shown in Fig. 3 that occurs near p = 1/8 (= 0.125) and which is common to a number of HTS cuprates and possibly to all. Certainly it is present in $La_{2-x}Sr_xCuO_4$, $YBa_2Cu_3O_{7-\delta}$, $Y_{0.8}Ca_{0.2}Ba_2Cu_3O_{7-\delta}$ and $HgBa_2CuO_{4+\delta}$, and in some variants of $La_{2-x}Sr_xCuO_4$ such as $La_{1.6-x}Nd_{0.4}Sr_xCuO_4$; T_c is fully suppressed there to zero. This is due to a competing AF *stripe phase*, where the parent spins and doped charges spatially separate into 1D or 2D stripes.[15] It has long been known that HTS tend to form such stripes but it is still not clear whether this is coincidental or crucial for SC.

The phase diagram shows the progression from long-range AF at low doping; through a region of short-range

AF order (the so-called pseudogap region below T^*); the onset of superconductivity at $p = 0.05$ rising to a maximum at optimum doping, $p = 0.16$, and the eventual decline in T_c in the *overdoped region*. In the heavily overdoped region, the cuprates progressively become more or less conventional metallic conductors, exhibiting many characteristics of the so-called Fermi liquid. Thus, there is a progressive crossover from strong correlations (magnetism) at low doping to weak or negligible correlations at high doping and an associated transition from insulating to metallic behaviour. A key question is whether there is a quantum phase transition at the point where T^* falls to zero at the critical doping $p_{crit} = 0.19$.[16] If so, then the occurrence of superconductivity and the dome-shaped $T_c(p)$ phase curve is due to strong quantum fluctuations above and near p_{crit}. There should be an insulator to metal transition at this point also (as observed[17]). Theory predicts that in this case the resistivity is linear-in-T above p_{crit} (as also observed) and the normal-state specific heat diverges logarithmically (not yet observed because SC conceals the normal state).[18] Despite dramatic improvements in the resolution of the many spectroscopies brought to bear on these questions the answers remain frustratingly elusive.

The above brief discussion outlines the electronic phase behaviour of the *hole-doped* cuprates. It is possible to dope *electrons* into some cuprates and thus explore the mirror image of the phase diagram shown in Fig. 3. Examples include $Nd_{1-x}Ce_xCuO_4$ and $Pr_{1-x}Ce_xCuO_4$, where Ce^{4+} is substituted on to a Nd^{3+} or Pr^{3+} site. Clearly, this is the converse of Sr^{2+} substitution on a La^{3+} site. However, the phase diagram for electron-doped cuprates is not quite the mirror image of that for hole-doped cuprates. Firstly, the AF domain is broader. This makes sense because the electrons dope on to Cu orbitals resulting in spin vacancies. This simply weakens the AF correlations. In the hole-doped cuprates, the holes are doped onto the O orbitals adding an extra spin and, thus, actually frustrating the AF correlations. Secondly, the SC dome in the electron-doped cuprates is more narrow, but there does appear to be a similar T^* line and putative quantum critical point lying at the centre of the dome[19] suggesting that the essential physics of the electron- and hole-doped cuprates is basically the same. A structural difference is that the hole-doped cuprates always possess somewhere in their structure an apical oxygen which is Jahn-Teller displaced away from the CuO_2 plane, whereas the electron-doped cuprates are restricted to structures with no apical oxygen. This surely means that the apical oxygen does not play a central role in the mechanism of electron pairing. However, the electron-doped systems all have relatively low T_c values and do not discount a secondary role for the apical oxygen through one of its associated phonon modes. Isotope substitution effects provide more light on this question, as discussed below.

Compositional Phase Diagrams

Compositional and structural phase diagrams play a key role in defining the synthesis conditions and doping prospects for perovskites in general and the cuprates are no exception. As noted, these materials are complex and often the observed structures reflect a compromise between the natural bond lengths in the block layer and those in the CuO_2 layers. This is the origin of the already-noted off-centre location of O atoms in the BiO layers of BSCCO.[7] Fig. 4 shows the domains of stability[20,21] of $YBa_2Cu_3O_{7-\delta}$, $Y_2Ba_4Cu_7O_{15-\delta}$, and $YBa_2Cu_4O_8$. The last compound is the low-temperature stable phase but the phase boundary is at sufficiently low temperature under ambient PO_2 that $YBa_2Cu_3O_{7-\delta}$ generally remains metastable as it is cooled. This is the case even if it is slow cooled, and this is fortunate as it is necessary to load in oxygen (reducing $\delta \rightarrow 0$) in order to achieve optimal SC properties. When $YBa_2Cu_3O_{7-\delta}$ is cooled to the dashed curve (marked O/T in Fig. 4) the $CuO_{1-\delta}$ chains have loaded to about 50% occupancy, *i.e.* $\delta \approx 0.5$, and the symmetry changes from tetragonal to orthorhombic in a 2nd order phase transition.[22,23] To the left of this line oxygen sites in the chain layer are randomly occupied and the structure is tetragonal, while to the right of the line oxygen atoms preferentially occupy the sites that form linear chain segments along the b-axis. This yields the orthorhombic phase. The tendency to form chains leads, in a well annealed sample, with $\delta \approx 0.5$, to alternating full and empty chains. It is also possible to achieve other ordered structures with an alternation of two full chains followed by one empty chain when $\delta \approx 0.33$, and alternation of one full chain followed by two empty chains when $\delta \approx 0.67$.

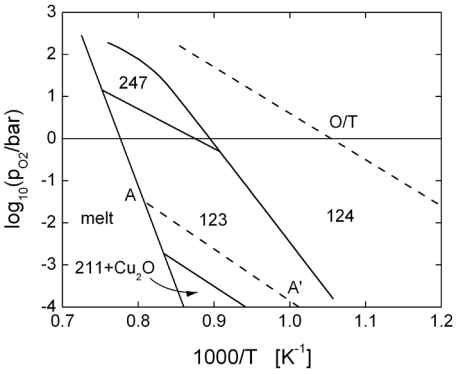

Fig. 4. The oxygen phase diagram for the Y/Ba/Cu/O system with Y-247 composition. The line O/T marks the orthorhombic/tetragonal transition in Y-123, the line A-A′ marks the phase boundary between Cu_2O and CuO and the line below this shows where Y-123 decomposes to $Cu_2O + Y_2BaCuO_5$ (referred to as 211).

Generally, elevated oxygen pressure (typically 60 bar O_2 pressure) is used to synthesize Y-124 or Y-247 in order to achieve temperatures sufficiently high to enable solid-state synthesis of these high-pressure phases. The horizontal solid line marks 1 bar of O_2 pressure and it cuts the Y-247 domain just above where it pinches off. In 1989, we discovered how to synthesize Y-247 in 1 bar of oxygen within this narrow domain (855-870 °C) by using $NaNO_3$ or KNO_3 as a reaction-rate enhancer. In the absence of some form of catalyst, the synthesis is just too sluggish (synthesis of Y-124 is harder still). Conveniently, the alkali evaporates during synthesis leaving pristine Y-247. We were surprised to discover the resultant material, $Y_2Ba_4Cu_7O_{15-\delta}$, was a 95 K superconductor (which we later improved to 97 K). What was particularly satisfying was that we were able to predict this narrow domain beforehand and our first attempt at 865 °C was success-

ful.[22,23] We subsequently found that the addition of Ag powder also acted as a suitable catalyst while remaining inert to the superconductor itself.

Phase diagrams like this are immensely useful. Of course, the melt line is important for the growth of single crystals by slow cooling across the melt boundary. We traversed samples of Y-124 from the stable region low down on the phase diagram ($PO_2 = 2 \times 10^{-4}$ bar) briefly into the Y-123 stability region to the left of the A-A′ line for a few seconds to a few minutes before returning to the stable Y-124 domain. The result was that Y-124 rapidly decomposed to Y-123 leaving precipitates of CuO within the structure. These precipitates are effective in pinning magnetic flux lines and the result was a 50-fold increase in critical current density.[23]

Fig. 5 shows the phase diagram for the stability of Bi-2212 and Bi-2223 where the overall composition is Bi-2223. Most importantly, this shows that the region of stability of Bi-2223 is very narrow and like Y-247 it pinches off, but in this case at higher pressure. The vertical line shows 1 bar O_2 pressure and here Bi-2223 is unstable. Any attempt to synthesize this in oxygen would have proved fruitless. Even in air (short solid vertical line) there is just a slender stability domain of about 5 °C where Bi-2223 can be synthesized. In early 1988, we discovered this narrow window and synthesized bulk Bi-2223, identified its composition and structure, and determined its behaviour as a function of oxygen content and doping. Bi-2223 became the material of choice for first generation HTS wires. Importantly, we recognised in our patents that Bi could be partially substituted by Pb because that subsequently proved to accelerate the reaction to the Bi-2223 phase sufficiently to make it a practical manufacturable process.[8] Moreover, reference to Fig. 5 shows that the synthesis range is much broader at low PO_2 and manufacturing is now typically carried out at $PO_2 = 0.077$ bar, indicated by the short vertical dashed line.

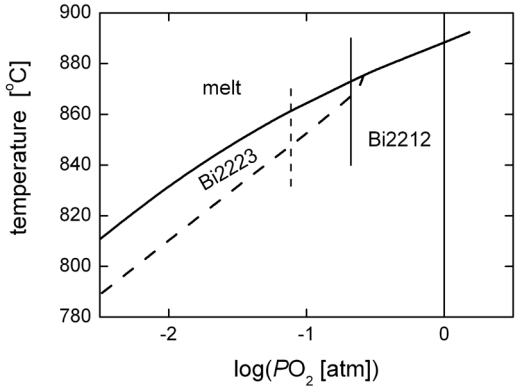

Fig. 5. The temperature/oxygen partial pressure phase diagram for the B/Sr/Ca/Cu/O system with Bi-2223 composition. The bold curve is the melting line while the short vertical solid line denotes ambient air where the stability range for $Bi_2Sr_2Ca_2Cu_3O_{10+\delta}$ is just 5 °C wide; the short vertical dashed line shows typical current manufacturing PO_2.

Systematics

The above basic ideas lay the foundation for exploring a number of systematic relationships that in principle allow the rational design of optimal high-T_c superconductors. The ensuing discussion does not just focus on maximising the value of T_c but, perhaps more importantly, addresses the practical issue of maximising the critical current density especially in an applied magnetic field.

Role of Multiple CuO_2 Layers

We have noted that the T_c value in an homologous series rises with the number of CuO_2 layers per unit cell up to $n = 3$ or 4 then falls again. To understand the role of multiple CuO_2 layers in controlling the value of T_c, it is useful to consider the standard BCS formula[2] for T_c, *viz.*:

$$T_c = 1.13h\nu_B \exp[-1/(N_0V)] \qquad \text{(Eq. 2)}$$

Here h is Plank's constant, N_0 the density of states (DOS), V the electron pairing interaction mediated by, *e.g.* phonons or magnons, and ν_B the characteristic frequency of the phonon or magnon. In conventional low-T_c superconductors the pairing is mediated by phonons so typically ν_B is the Debye frequency. The key point here is that T_c is governed exponentially by the DOS and, thus, the presence of a van Hove singularity (vHs) associated with the two-dimensionality can have a dominant effect since N_0 diverges at the vHs. This probably plays a central role in causing the very high T_c values in the layered cuprates.

Let us consider what happens when the doping (the hole concentration, p) is increased. In the cuprates, the pairing is almost certainly mediated by magnetic interactions and, as noted, these diminish as p increases. Thus, both ν_B and V decrease with increasing doping.[24] This would suggest that the highest T_c values might be achieved at low doping. However, in single-layer cuprates the vHs is located right at the far edge of the SC domain shown in Fig. 3 around $p \approx 0.27$. This is where the magnetic interactions are weakest and it is not surprising that $T_{c,max}$ is low for these. On the other hand, a bilayer system has two degenerate orbitals that are split by the (weak) coupling between them into a lower bonding (B) and a higher antibonding (AB) orbital. This splits the vHs with the AB vHs moving to lower doping,[25] where the magnetic interactions are stronger, and so T_c rises, and quite dramatically so. A trilayer system splits the three-fold degenerate orbitals into three levels which push one of the vHs to even lower doping and hence still higher T_c.

This cannot continue indefinitely because the block layer transfers a fixed quantity of doped charge into the CuO_2 layers. As the number of CuO_2 layers is increased the doped charge becomes increasingly diluted.[14] If we think of each layer as having its own phase diagram as shown in Fig. 3 then, eventually, all the layers become underdoped and T_c declines. Worse still, once there are more than two CuO_2 layers they are no longer structurally and electronically equivalent. A three-layer cuprate has two identical outer layers and a different inner layer. This inner layer tends to be less doped than the outer layers.[26,27] Ideally, one would like to achieve equal doping in all layers so that all could simultaneously be optimized. In principle, this could be done by judicious site substitution or some form of structural distortion, but these might prove difficult to achieve and no-one has yet explored this as a computational chemistry problem. Interestingly, the applica-

tion of pressure squeezes further charge transfer from the block layers to the CuO_2 planes – it is an indirect means of systematically increasing the doping. By applying pressure to three-layer cuprates such as $Bi_2Sr_2Ca_2Cu_3O_{10+\delta}$,[28] and $Tl_2Ba_2Ca_2Cu_3O_{10+\delta}$,[29] one finds that T_c rises to a maximum as the outer layers reach their optimum doping, and then it falls for an interval where the inner layer is underdoped and the outer layer is overdoped. Then T_c rises again as the inner layer approaches optimum doping, and it rises much higher than the first maximum. One expects that at high enough pressure both inner and outer layers are overdoped. Clearly, (i) the inner layer (lacking apical oxygens) has a significantly higher intrinsic T_c value than the outer layers[28,30,31] (see T_c *Correlations*) and (ii) if the doping were uniform across all three layers then higher T_c could be obtained. By no means have we found the best HTS superconductors yet.

Role of Block-Layers

As noted, between the bilayers and trilayers in Figs. 1 and 2 lies an essentially inert layer, referred to as the *block layer*. This acts firstly as a charge reservoir that provides the source of the doped charge in the CuO_2 layers, either through oxygen non-stoichiometry or altervalent cation substitution. The block layer provides charge compensation for the doped electrons or holes such that the overall charge is neutral, as it must be. Secondly, the block layer provides a substrate that determines the Cu-O bond-length. This bond length plays an important role in controlling the thermodynamic stability (see *Thermodynamic Stability*) and also the maximum T_c value (see T_c *Correlations*). Adjacent multilayers are weakly coupled by quantum mechanical *inter*layer tunnelling of electron pairs across the block layer, while the multilayer itself is quite strongly coupled *intra*layer. These couplings can be probed by, for example, infrared spectroscopy and they play an important role in determining the strength of the superconducting state.

Other high-T_c compounds discovered after the cuprates also possess this weakly-coupled layered structure, including MgB_2 and, more recently, the iron pnictides (layered iron arsenic compounds). Therefore, it seems a general conclusion that this quasi-two-dimensionality is important – it imposes the van Hove singularity, which introduces a very large DOS when the doping level is close to the vHs. But, there is a trade-off here because a purely 2D electronic system cannot be a superconductor. Indeed, it is clear that most cuprate superconductors are too two-dimensional and some coupling along the *c*-axis is definitely desirable, both to increase T_c and to increase the critical current in a magnetic field. This can be quantified through the so-called *irreversibility field*. In the presence of a magnetic field, flux will concentrate into discrete tubes of exactly one flux quantum, given by $h/2e$, where e is the electronic charge. The field outside these tubes of flux is suppressed to zero by circulating supercurrents and the composite object is referred to as a *vortex*. When a current passes through the superconductor there is a lateral force on the vortex (the Lorentz force) which is normal to the field and the current flow. If the vortex should move under this force the process is dissipative and, though we have a superconductor, it does not display zero resistance. Great efforts are expended, therefore, to control the microstructure to pin these vortices through various precipitates and defects.[21] In a 3D system, a vortex is continuous along its length and more or less rigid. However, in a layered quasi-2D system the vortex is a stack of current loops within each CuO_2 plane. These are referred to as *pancake vortices* and they can decouple from each other if the field is too high. You may pin one section of the vortex but adjacent sections can decouple and slide under the Lorentz force. Therefore, pinning is a much greater challenge in layered high-T_c superconductors. This decoupling occurs at a critical field known as the irreversibility field, H^*. If $H < H^*$ then the pancakes are strongly coupled and zero DC resistance is accomplished, but if $H > H^*$ then decoupling occurs and the superconductor becomes resistive. Clearly, one wants to increase the coupling across the block layer to ensure that H^* is as high as possible.

This coupling is governed by quantum mechanical tunnelling and, therefore, varies exponentially with the thickness, t_b, of the block layer. A simple calculation shows that $H^* \propto \exp(-t_b/\xi)$, where ξ is a fixed characteristic length. Fig. 6 shows $\ln(H^*)$ plotted against t_b for many different cuprates[32] and the expected relationship is well satisfied. There are a number of subtleties present in this plot. Firstly, H^* varies strongly with doping, so that all values are compared at the same doping state, namely optimal doping where $p = 0.16$ and T_c maximizes. Secondly, the true block layer spacing for Y-123 and Y-247 is shown by the open symbols that definitely do not fit the correlation. But, as noted, the chain layers in both of these compounds are metallic and superconducting by proximity effect, so the block-layer spacing, over which the coupling must extend, is the plane-to-chain distance not the plane-to-plane distance. The former is exactly half the latter and it is these coupling lengths that are used in plotting the solid data points.

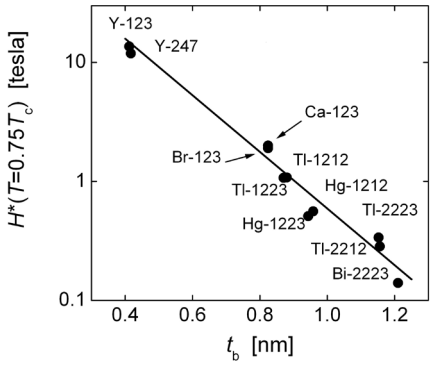

Fig. 6. The irreversibility field H^* at 0.75 T_c for optimal doped cuprates as a function of block-layer spacing, t_b. Ca-123 denotes $Y_{0.8}Ca_{0.2}Ba_2Cu_3O_{6.61}$ and Br-123 denotes $YBa_2Cu_3O_{6.2}Br_{0.8}$; for Y-123, t_b is taken to be 0.42 nm, the chain-to-plane distance.

This not only confirms the basic correlation shown in Fig. 6 but provides indirect evidence for proximity-induced SC on the chains. More rigorous studies using muon spin relaxation to probe the superfluid density in these materials confirms this picture.[33] As a test of this interpretation, the figure also shows H^* for Ca-doped Y-123 and for Br-

doped Y-123 where the chains have been fully disrupted while retaining the same optimal doping state. Here, the effective block-layer distance is now the plane-to-plane distance and the value of H^* is reduced accordingly, in keeping with the overall correlation. What is notable in this figure is the fact that Bi-2223, which forms the first generation HTS wire technology, has the poorest irreversibility field of all the cuprates, while Y-123 which forms basis of second generation HTS wire technology has the best. This is a primary motivation for implementing this material – its critical current in a magnetic field is superior to all other HTS except Y-247.

Bond-Valence Sums

As noted, there are several HTS cuprates where the doping value, p, is directly calculable from the composition. Two examples will suffice. In the case of $La_{2-x}Sr_xCuO_4$ it is simple to see that $p = x$. For $Y_{1-x}Ca_xBa_2Cu_3O_6$,where the chain layer has been fully deoxygenated and the chain coppers are Cu^{1+}, then $p = x/2$, since the doped charge x is distributed over two CuO_2 layers. However, for most other systems the doping state is not directly calculable because of oxygen and cation non-stoichiometry. A simple example is $YBa_2Cu_3O_{7-\delta}$, where the doped charge 2(1-δ) is uncertainly distributed over the separate chain and plane coppers. In this case, the use of bond valence sums has proved useful in fairly accurately determining p. The bond valence sum (BVS) about a Cu atom within a structure is given by:[34]

$$V_{Cu} = \Sigma_j \exp [- (r_j - r_0)/0.37] \qquad \text{(Eq. 3)}$$

where the sum is over the nearest-neighbour oxygens, r_j is the bond length for each neighbour and r_0 is a characteristic length for the Cu-O pair. The value of r_0 for many cation-anion pairs has been tabulated by Brown.[34,35] Such BVS values have been used to estimate the doping state as $p = V_{Cu} - 2$ or, indeed, the valence of any of the relevant cations is given by its BVS. However, in view of the fact that the doped holes reside dominantly on the oxygen orbitals, it seemed to the author that one needs also to include oxygen BVS to determine the overall doped charge which can be distributed over both Cu and O orbitals. An expression similar to Eq. 3 is used for the oxygen BVS, V_O, except that the sum now includes all nearest-neighbour Cu-O pairs as well as Ba-O and Y-O pairs. The total doping state was estimated as:[36]

$$p \approx V\_ = 2 + V_{Cu} - V_{O2} - V_{O3} \qquad \text{(Eq. 4)}$$

where O2 is the oxygen residing between two coppers aligned in the *a*-direction and O3 is the oxygen residing between two coppers aligned in the *b*-direction. This also allows the definition of another composite BVS, which is a nominal measure of the relative distribution of doped charge between the oxygen and copper orbitals, namely:[36]

$$V_+ = 6 - V_{Cu} - V_{O2} - V_{O3} \qquad \text{(Eq. 5)}$$

This second parameter is extremely useful and also acts as a measure of stress in the plane – negative values indicate a compressive stress, while positive values indicate a tensile stress.

Polycrystalline samples of $Y_{1-x}Ca_xBa_2Cu_3O_{7-\delta}$ were synthesized and structural refinements were performed on neutron diffraction data collected at the Argonne National Laboratory.[37] From the bond-lengths, BVS values were calculated and values of V_ calculated from Eq. 4 are plotted in Fig. 7 as a function of δ for calcium contents of x = 0, 0.1 and 0.2. These show an initial linear region followed by a plateau as δ → 1. The plateau can be understood from the fact that when δ = 1 all the chain coppers are Cu^{1+}. When δ is reduced fractionally below unity the oxygens in the chain layer are dilute and isolated such that each incorporated oxygen merely changes the valence of the two adjacent coppers to Cu^{2+}. As long as no chain segments are formed, there is full charge balance in this process and no charge is transferred to the CuO_2 planes. Here p is independent of δ. Only when chain segments form at higher oxygen concentration is there residual charge. This is transferred to the planes and p starts to rise. As noted, when δ is exactly 1 the value of p is exactly $x/2$. In Fig. 7 this is very nearly satisfied by $V\_$ and we believe that all estimates of p in Fig. 7 should be rigidly shifted by just +0.01.

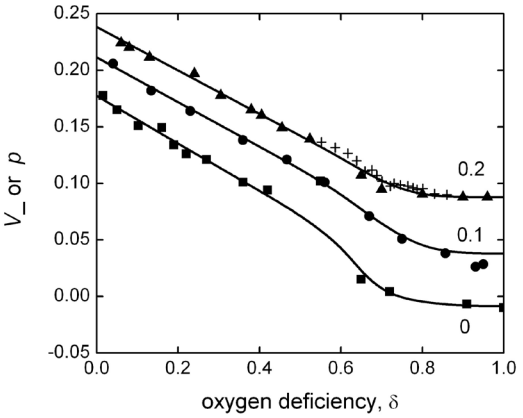

Fig. 7. The variation of p, estimated from the BVS parameter $V\_$, with oxygen deficiency in $Y_{1-x}Ca_xBa_2Cu_3O_{7-\delta}$. Values of x are shown for each curve; near full oxygenation the curves are linear with slope 0.21 holes/oxygen while as δ → 1 the hole density is independent of δ; actual values of p are probably 0.01 larger in all cases.

T_c Correlations

This BVS procedure allows an estimate of the doping state of the rather complex $Y_{1-x}Ca_xBa_2Cu_3O_{7-\delta}$ system that has become a standard in the field. When we consider the value of V_+ as a function of δ, it turns out to be constant across the entire doping range. This is useful because it means that $V\_$ and V_+ are orthogonal with respect to oxygen doping. On the other hand, it is a very different story when we consider V_+ across a range of different HTS cuprates. Fig. 8 shows $T_{c,max}$ plotted against V_+ for 33 different cuprates. There is a remarkable correlation that shows $T_{c,max}$ trending steadily upwards as the CuO_2 planes are brought under increasing tensile stress and the doped charge is displaced increasingly onto the O_{2p} orbitals. The uppermost four data points are for trilayer cuprates where we have the option of calculating V_+ for the inner plane or for the outer planes. The data plotted are for the inner plane and if V_+ is calculated for the outer planes the data points lie deep on the compressive side, completely un-

correlated with the other cuprates.[32] It is clear, therefore, that it is the inner planes that determine the magnitude of $T_{c,max}$ even though, as noted, the inner plane is well short of optimal doping.[28]

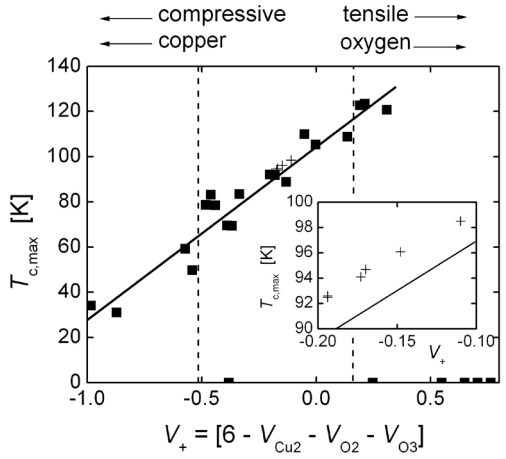

Fig. 8. The correlation of $T_{c,max}$ with the bond valence sum parameter V_+. Negative values of V_+ correspond to a compressive in-plane stress and holes tending to reside more on Cu 3d orbitals while positive values correspond to a tensile in-plane stress and holes tending to reside more on oxygen 2p orbitals.

The clear implication of this correlation is that a strategy to increase T_c would include stretching the Cu-O bond by, for example, substituting larger cations. However, V_+ is a more complex measure than merely that of Cu-O bond length – it may, *e.g.* be increased by moving the apical oxygen further away. Consistent with this, the inner layer in trilayer systems has no apical oxygen at all and this displays a higher intrinsic T_c value than do the outer layers which have an apical oxygen. Nonetheless, the simple approach of substituting larger equivalent cations seems to be well borne out. Fig. 8 also shows data (crosses) for six different $RBa_2Cu_3O_7$ where R is a lanthanide rare-earth element ranging from La to Yb;[38] the inset enlarges this region. On progressing across the lanthanide series the ion size progressively contracts. At the same time $T_{c,max}$ is progressively diminished. In the figure, this progression can be seen to follow the broader correlation with essentially the same slope. In similar fashion, $T_{c,max}$ in $Bi_2Sr_{1.6}R_{0.4}CuO_6$ is found to systematically decrease as R decreases. Based on these considerations, given that the highest T_c thus far observed is found in $HgBa_2Ca_2Cu_3O_8$ ($T_{c,max}$ = 134 K), it is to be expected that this record would be further raised in the material $HgRa_2Ca_2Cu_3O_8$ where barium is replaced by the larger radium. The complications of radioactivity have prevented any attempts to synthesize this material!

Thermodynamic Stability

There is an unexpected link between the above ideas and the thermodynamic stability of the HTS cuprates at different temperatures and oxygen partial pressures, PO_2. We found that all those cuprates with a good lattice match between the block layer and the CuO_2 layer, such that the CuO_2 layer was under neither tension nor compression, decomposed on the stability boundary between CuO and Cu_2O. This is the line A-A′ shown in Fig. 4, where $\log_{10}(PO_2)$ is plotted *vs* $1000/T$ (K^{-1}), and it is the limit of stability of Cu^{2+} relative to Cu^{1+}. For these unstressed cuprates it is the CuO_2 layer that determines the stability. This includes all the cuprates found between the two vertical dashed lines of Fig. 8. On the other hand, those compounds where there is a mismatch between the block layer and the CuO_2 plane, either in tension or compression, remain stable to much higher temperatures than the A-A′ boundary. For these, it is the block layer that determines the thermodynamic stability and this includes all cuprates which lie outside the two vertical dashed lines of Fig. 8. These limitations are important for determining the upper limits for annealing the cuprates. They can also be used as a guide to annealing conditions suitable for causing partial decomposition as is often needed to control the microstructure for enhanced flux pinning.

The Contrary Effects of Pressure

We close this section by noting the anomalous effects of pressure on T_c. The correlation summarised in Fig. 8 would suggest that any means by which the lattice can be expanded will increase T_c and, conversely, any means by which it is compressed will decrease T_c. Hence one would expect the application of external pressure to reduce T_c. In fact it does the opposite.

We have measured the pressure dependence of T_c in $YBa_2Cu_4O_8$ using a *home-built* beryllium-copper clamp cell in a SQUID magnetometer.[39] Additionally, the sample was oxygen isotope exchanged by extended annealing at 750 °C in ^{18}O and then, after measurements, back exchanged again in ^{16}O. Fig. 9 shows T_c *vs* P for the two isotope-exchanged samples. In both cases T_c rises very rapidly – at a rate of +5.24 K/GPa for ^{18}O and +5.4 K/GPa for ^{16}O. A slight negative curvature is also evident and it is known that $T_c(P)$ reaches a maximum of 106 K at about 10 GPa before falling at higher pressure. As noted, this behaviour is puzzling because Fig. 8 suggests that such a compressive stress should *decrease* T_c. Indeed, given the typical compressibility of the cuprates, converting the ion-size effects noted in Section 4.4 into an effective internal (or chemical) pressure, one would expect T_c to *fall* at 5 or 6 K/GPa. The magnitude is right but the sign is wrong.

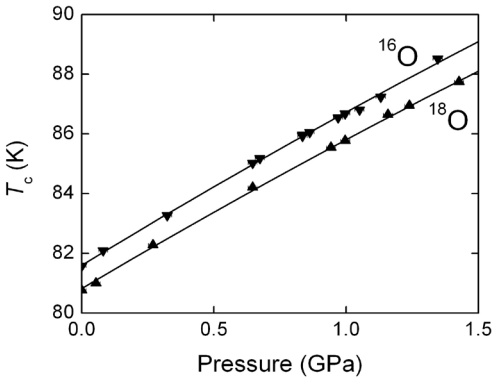

Fig. 9. The pressure dependence of T_c for $YBa_2Cu_4O_8$ where all oxygens in the compound are exchanged for either ^{16}O or ^{18}O isotopes. In both cases T_c rises very rapidly – at +5.24 K/GPa for ^{18}O and +5.4 K/GPa for ^{16}O; reproduced from ref. 39.

This contradiction is a crucial observation and it is the author's view that its resolution will lead to a major advance

in our understanding of HTS. The underlying issues and possible solutions are beyond the scope of the present discussion. Nonetheless, it is likely that pressure suppresses fluctuations and thereby increases T_c, while decreasing ion-size probably distorts the Fermi surface, shifting the location of the vHs to higher doping – this would decrease the DOS and thereby reduce T_c. Again, quantum chemistry calculations could shed much light on this hypothesis. The impact of pressure and ion size on other physical properties, such as the magnetic correlations and pairing interactions, will also play a significant role and research efforts should be directed towards disentangling all these competing behaviours.

Substitution Chemistry

The versatility of the cuprates lies in their diversity of structural families and their propensity for forming homologous series. It also lies in their ability to accommodate a wide range of atomic substituents into the parent compounds. These may be of various sorts generally separable into (i) substitutions in the block layer and (ii) substitutions in the CuO_2 layer. The former may be of the same valence and, therefore, impact only through ion-size effects or they may be altervalent and change the doping state (as well as impose ion-size effects). In either case their impact is incremental. The substitutions into the CuO_2 layers are generally strongly deleterious towards superconductivity.

Doping

There are two main reasons for altering the doping state of HTS cuprates: firstly, in order to optimise the intrinsic superconducting properties and, secondly, to explore the physical and chemical properties as a function of doping across the entire phase diagram in order to probe the fundamental mechanisms underlying their normal and superconducting state. The easiest route is to change the oxygen content. Thus, $YBa_2Cu_3O_{7-\delta}$ may be shifted from the undoped insulating state ($p = 0$, $\delta = 1$) to the onset of superconductivity ($p = 0.05$, $\delta \approx 0.6$), to optimal doping ($p = 0.16$, $\delta \approx 0.13$), to critical doping where the pseudo-gap vanishes ($p = 0.19$, $\delta \approx 0$) simply by varying the oxygen content. Typically, we anneal the sample to equilibrium in a flow of $O_2 + N_2$ gas at fixed temperature in a vertical furnace; then, using a magnetic release mechanism, quench directly into liquid nitrogen in order to freeze in the desired oxygen stoichiometry. The physical properties may then be explored and the process repeated to progress across the phase diagram. The so-called *critical doping state* is the desired target for applications because this is where the superfluid density and critical current density is maximized. As noted, the sample is a little overdoped relative to optimal doping where T_c is maximized, but this is a small sacrifice in relation to the very substantial improvement in practical properties, especially performance in a magnetic field, that is achieved by this rather small increase in doping. We have patents to cover this process of fine tuning.

Often one may wish to extend the doping in $YBa_2Cu_3O_{7-\delta}$ to higher levels in order to explore the more deeply overdoped region. This cannot be done by further increases in oxygen content. Instead, one typically has to resort to altervalent substitution where Ca^{2+} is substituted for Y^{3+} in the composition $Y_{1-x}Ca_xBa_2Cu_3O_{7-\delta}$. The solubility limit is around $x = 0.2$ and, even here, the synthesis is tricky, requiring reactions close to the melting point, leaving a window of just a few degrees C. In this way, a maximal doping of $p \approx 0.24$ can be achieved with T_c reduced to about 45 K in the overdoped region. It is somewhat frustrating that most substitutions in HTS cuprates cannot shift far away from optimal doping. There are a few exceptions, such as $La_{2-x}Sr_xCuO_4$ where the doping level can be changed from $p = x = 0$ to $p = x = 0.3$. But this tendency for as-synthesized HTS to sit somewhere generally near optimal doping and to resist doping far away from this is rather thought-provoking and suggests a close relationship between structural stability and the occurrence of superconductivity. In particular, it may be that T_c is optimized close to a structural instability and, indeed, there is a strong tendency in these systems to phase separate or to exhibit various forms of electronic and structural inhomogeneity. Avoidance of a vHs is likely to play a role here.

The above substitution of Ca^{2+} for Y^{3+} is a hole-doping substitution, which in general can be promoted by using a low oxygen partial pressure in the synthesis atmosphere. Electron-doping substitutions, *e.g.* La^{3+} for Ba^{2+}, are generally promoted using a high oxygen partial pressure. It is also possible to co-dope Ca^{2+} for Y^{3+} and La^{3+} for Ba^{2+}, resulting in the compound $Y_{1-x}Ca_xBa_{2-x}La_xCu_3O_7$. As may be expected, the doping does not alter but disorder is progressively increased with increasing x. Surprisingly, disorder has little effect – even the superfluid density, which is very sensitive to pair-breaking, is barely diminished.[40]

These types of altervalent substitutions can be used across the wide variety of HTS cuprates to increase or decrease the doping state, although one often encounters narrow solubility limits, as discussed. Just one further example is needed to establish the pattern. The compound $Bi_2Sr_2CaCu_2O_{8+\delta}$ is limited to a narrow range around optimal doping by varying the oxygen content as described by the value of δ. The doping state may be reduced (electron doping) by substituting Y^{3+} for Ca^{2+} or increased by substituting Pb^{2+} for Bi^{3+}. Furthermore, there is a tendency for some Bi^{3+} to substitute on the Sr^{2+} site as noted, even in the pure compound; this is an electron doping substitution. Using the above guidelines this can be suppressed by synthesizing under low oxygen partial pressure.

Ion-Size Effects

It is the author's view that ion-size effects provide an important (but as yet relatively unused) key to unravelling the physics of HTS. Therefore they deserve considerable discussion. A productive approach would be to explore non-doping homovalent substitutions such as Ca^{2+} for Sr^{2+} (smaller) or Ba^{2+} for Sr^{2+} (larger), or substitution across the lanthanide series for Y^{3+}. The questions to be asked are: (i) What is the effect on key superconducting parameters? (ii) What is the effect on the pseudo-gap temperature, T^*, and energy, E_g? (iii) If pairing originates in the magnetic correlations, what is the effect on the magnetic exchange energy J? (iv) Do these substitutions shift the

van Hove singularity to lower or higher doping? (v) How do these shifts correlate with the effects of external pressure? (v) How do they correlate with the strain effects of lattice mismatch in epitaxial thin films on single-crystal substrates? and (vi) How do all these correlate with T_c? This offers a rich arena of on-going studies on HTS utilising such techniques as Raman scattering, specific heat, NMR, electron tunnelling and electron transport – magnetoresistance, Hall effect and thermoelectric power.

Isotope Exchange

Conventional superconductors derive their Cooper pairing from the interaction of electrons and phonons. This was first evidenced by the observed reduction in T_c when an element was replaced by a heavier isotope. Eq. (2) shows that T_c is proportional to the characteristic frequency, ν_B, of the pairing correlation and in conventional superconductors the pairing is mediated by phonons. So ν_B is the Debye frequency that varies inversely as the square root of the elemental mass. Thus, we have the isotope effect coefficient:

$$\alpha \equiv -(\Delta T_c/T_c)/(\Delta M/M) = 0.5 \qquad \text{(Eq. 6)}$$

Here, α is the ratio of the fractional change in T_c to the fractional change in isotopic mass, and it takes the value 0.5 because of the square root dependence of the Debye frequency on mass. In 1950, precisely this relationship was found in the case of the isotopes of Sn[41] and this was the crucial guide that ultimately established the BCS theory of SC.

It is widely believed that the HTS cuprates derive their pairing interaction from magnetic correlations, and here the large value of T_c would be partly established by the very large magnetic energy scale given by J = 1390 K (expressed in temperature units), *cf.* the Debye temperature of about 270 K. This being the case, one would not expect an isotope effect. However, Fig. 9 shows that there is an oxygen isotope effect indeed, albeit small – α is about 0.075, rather less than the value of ½ given in Eq. 6. Moreover, α grows dramatically with underdoping and possibly diverges at p = 0.05 where SC disappears.[42] We understand this divergence as arising from the pseudo-gap which competes with SC.[42] Thus, we conclude that there is a residual underlying isotope effect but it is small, suggesting that perhaps both phonons and magnetism play a role in forming Cooper pairs, though phonons are (probably) the junior partner. Site selective isotope exchange shows that it is only the oxygens in the CuO_2 plane that contribute an isotope effect.[43] Apical oxygens thus play little or no role in SC pairing.

Summary: The Ideal TS Superconductor

Drawing all the above thoughts together we can say, in conclusion, that there are a number of clear guidelines to establish the ideal cuprate superconductor. Firstly, $T_{c,max}$ will be maximized by stretching the lattice as much as possible through appropriate atomic substitutions and/or lattice mismatch in epitaxial thin films. This is opposite to the effect of applying an external pressure, probably because the latter primarily works towards suppressing fluctuations. In order to suppress fluctuations under ambient conditions, it is beneficial to enhance the interlayer coupling, probably best achieved through metallizing one of the interlayers in the block layer. The Y-123 and Y-247 class of superconductor achieve this naturally via the chain layer(s) that are metallic and in which superconductivity seems to be induced by the well-known proximity effect. To achieve the highest critical current density, it is necessary to tune to critical doping (p_{crit} = 0.19) rather than optimal doping (p = 0.16). However, if the material is to be operated at low temperature, and because the irreversibility field, H^*, continues to steepen with overdoping, it could be beneficial to overdope a little beyond p_{crit}. Again, H^* is increased by increasing the interlayer coupling either by metallizing an interlayer or by reducing the block-layer spacing t_b. This can be achieved by removing one or more layers within the block layer, or by reducing ion sizes within the block layer. The latter would have the effect of *reducing* $T_{c,max}$ so one is left with a compromise between T_c and critical current density. Of these, current density is probably the most important. It is possible to remove layers from the block layer and, indeed, this is the cause of the increased value of H^* seen in Fig. 6 in progressing from Tl-2212 to Tl-1212 and from Tl-2223 to Tl-1223, where one of the TlO layers has been removed.

By means of judicious site substitution one ought to be able to secure a more even distribution of charge in trilayer HTS so that both inner and outer layers can be optimized simultaneously. This could result in very large increases in $T_{c,max}$. We also have much to learn about how to shift the vHs to lower doping in order to capture a larger DOS. But the ideal HTS would be the so-called infinite-layer compound where every second layer is a CuO_2 layer. Such a system would be very strongly coupled. The intervening divalent alkali earth should be as large as possible and, therefore, should be Ba^{2+} (if we abandon Ra^{2+}). Then it needs to be doped, preferably with a large monovalent ion such as K^+. This leads us to $Ba_{1-x}K_xCuO_2$ or even $Ba_{1-x}Rb_xCuO_2$ where x = 0.19. This cannot be synthesized under ambient pressure but possibly under high-pressure/high-temperature synthesis, or preferably through physical deposition of thin films. We shall see.

References

1. Bednorz J. G.; Muller, K. A. *Z. Phys.* **1986**, *B 64*, 189.
2. Bardeen, J.; Cooper, L. N.; Schrieffer, J. R. *Phys. Rev.* **1957**, *106*, 162, *108*, 1175.
3. Tallon, J. L.; Bernhard, C.; Binninger, U.; Hofer, A. *et al. Phys. Rev. Lett.* **1995**, *74*, 1008.
4. Tallon, J. L.; Pooke, D. M.; Buckley, R. G.; Presland, M. R.; Blunt, J. *Phys. Rev. B.* **1990**, *41*, 7220.
5. Tallon, J. L. Buckley, R. G.; Gilberd, P. W.; Presland, M. R.; *et al. Nature* **1988**, *333*, 153.
6. McElroy, K.; Lee, J.; Slezak, J. A.; Lee, D.-H. *et al. Science* **2005**, *309*, 1048.
7. Stoto, T.; Pooke, D.; Forro, L.; Kishio K. *Phys. Rev.* **1996**, *B54*, 16147.
8. Tallon, J. L. Buckley, R. G.; Gilberd, P. W.; Presland, M. R. *Physica* **1989,** *C 58*, 247.
9. Eisaki, H.; Kaneko, N.; Feng, D. L.; Damascelli, A. *et al. Phys. Rev.* **2004**, *B 69*, 064512.
10. Sheng, Z. Z.; Hermann**,** A. M. *Nature* **1988**, *332*, 55, *60*, 937.

11. Putilin, S. N.; Antipov, E. V.; Chmaissem, O.; Marezio, M. *Nature* **1993**, *362*, 226.
12. Tallon, J. L. Williams, G. V. M.; Flower, N. E.; Bernhard, C. *Physica* **1997**, *C282-287*, 236.
13. Niedermayer, Ch.; Bernhard, C.; Blasius, T.; Golnik, A. *et al*. *Phys. Rev. Lett*. **1998**, *80*, 3843.
14. Presland, M. R., Tallon, J. L. Buckley, R. G.; Liu, R. S.; Flower, N. E. *Physica* **1991**, *C176*, 95.
15. Tranquada, J. M.; Sternlieb, B. J.; Axe, J. D.; Nakamura, Y.; Uchida, S. *et al*., *Nature* **1995**, *375*, 561.
16. Tallon, J. L.; Loram, J. W.; Williams, G. V. M.; Cooper, J. R., *et al. Phys. Stat. Solidi* **1999**, *(b)215*, 531.
17. Boebinger, G. S.; Ando, Y.; Passner, A.; Kimura, T. *et al. Phys. Rev. Lett.* **1996**, *77*, 5417.
18. Trovarelli, O.; Geibel, C.; Mederle, S.; Langhammer, C. *et al. Phys. Rev. Lett.* **2000**, *85*, 626.
19. Alff, L.; Krockenberger, Y.; Welter, B.; Schonecke, M. *et al. Nature* **2003**. *442*, 698.
20. Pooke, D. M.; Buckley, R. G.; Presland, M. R.; Tallon, J. L. *Phys. Rev.* **1990**, *B41*, 6616.
21. Tallon, J. L.; Pooke, D. M.; Buckley, R. G.; Presland, M. R. *et al. Appl. Phys. Lett.* **1991**, *59*, 1239.
22. Tallon, J. L. *Phys. Rev.* **1989**, *B39*, 2784.
23. Tallon, J. L.; Schuitema, A. H.; Tapp, N. J. *Appl. Phys. Lett.* **1998**, *52*, 507.
24. Storey, J. G.; Tallon, J. L.; Williams, G. V. M. *Phys. Rev.* **2007**, *B6*, 174522.
25. Kaminski, A.; Rosenkranz, S.; Fretwell, H. M.; Norman, M. R. *et al*. *Phys. Rev.* **2006**, *B73*, 174511.
26. Trokiner, A.; Le Noc, L.; Schneck, J.; Pougnet, A. M. *et al*. *Phys. Rev.* **1991**, *B44*, 2426.
27. Statt; B. W.; Song, L.M. *Phys. Rev*. **1993**, *B48*, 3536.
28. Chen X.-J.; Struzhkin, V. V.; Yu, Y.; Goncharov, A. F. *et al*. *Nature* **2010**, *466*, 950.
29. Jover, D. T.; Wijngaarden, R. J.; Griessen, R.; Haines, E. M. *et al. Phys. Rev.* **1996**, *B* 54, 10175.
30. Haines, E. M.; Tallon, J. L. *Phys. Rev*. **1992**, *B45,* 3172.
31. Ideta S; Takashima K; Hashimoto M; Yoshida T. *et al*. *Phys. Rev. Lett*. **2010**, *104*, 227001.
32. Tallon, J. L. Williams, G. V. M.; Bernhard, C.; Pooke, D. M., *et al. Phys. Rev.* **1996**, *B53*, R11618.
33. Tallon, J. L.; Bernhard, C.; Binninger, U.; Hofer, A. *et al. Phys. Rev. Lett.* **1995**, *74*, 1008.
34. Brown, I. D. *J. Sol. State Chem*. **1989**, *82*, 122.
35. Brown, I. D.; Altermatt, D. *Acta Cryst*. **1985**, *B41*, 244.
36. Tallon, J. L. *Physica* **1990**, *C168*, 85.
37. Tallon, J. L. Bernhard, C.; Shaked, H.; Hitterman; R. L.; Jorgensen, J. D. *Phys. Rev.* **1995**, *B51*, R12911.
38. Williams; G. V. M.; Tallon, J. L. *Physica* **1996**, *C258*, 41.
39. Suresh, N.; Storey, J. G.; Williams, G. V. M.; Tallon, J. L. *Phys. Rev.* **2008**, *B78*, R100503.
40. Tallon, J. L.; Bernhard, C.; Niedermayer, Ch. *Supercon. Sci. Tech.* **1997**, *10*, A38.
41. Allen, W. D.; Dawton, R. H.; Lock, J. M.; Pippard, A. B.; Shoenberg, D. *Nature* **1950**, *166*, 1071.
42. Williams; G. V. M.; Tallon, J. L.; Quilty, J.; Trodahl, H. J.; Flower, N. E. *Phys. Rev. Lett.* **1998**, *80*, 377.
43. Khasanov, R.; Shengelaya, A.; Morenzoni, E.; Angst, M. *et al. Phys. Rev.* **2003**, *B68*, 220506.